sustainability

MDPI

Article

Identifying the Areas Benefitting from the Prevention of Wind Erosion by the Key Ecological Function Area for the Protection of Desertification in Hunshandake, China

Yu Xiao [1,2,*], Gaodi Xie [1,2], Lin Zhen [1,2], Chunxia Lu [1,2] and Jie Xu [1,2]

1 Institute of Geographic Sciences and Natural Resources Research, Chinese Academy of Sciences, Beijing 100101, China; xiegd@igsnrr.ac.cn (G.X.); zhenl@igsnrr.ac.cn (L.Z.); lucx@igsnrr.ac.cn (C.L.); xuj.16b@igsnrr.ac.cn (J.X.)

2 University of the Chinese Academy of Sciences, Beijing 100049, China

* Correspondence: xiaoy@igsnrr.ac.cn; Tel.: +86-10-6488-8157

Received: 30 August 2017; Accepted: 7 October 2017; Published: 12 October 2017

Abstract: Research on the spatial flow of ecosystem services can help to identify the spatial relationships between service-providing areas (SPAs) and service-benefitting areas (SBAs). In this study, we used the Hybrid Single-Particle Lagrangian Integrated Trajectory (HYSPLIT) model to stimulate the flow paths of the wind erosion prevented by ecosystems in Hunshandake, China. By interpolating these paths, the SBAs were identified, and their benefits in terms of land cover, population, and Gross Domestic Product (GDP) were determined. The results indicated that the flow paths mostly extended to the eastern part of the study area, and the estimated cover of the SBAs was 39.21% of the total area of China. The grid cells through which many ($\geq$10%) of the trajectories passed were mainly located in the western part of north-eastern China and the eastern part of northern China. The benefitting population accounted for 74.51% of the total population of China, and the GDP was 67.11% of the total in 2010. Based on this research, we described a quantitative relationship between the SPAs and the SBAs and identified the actual beneficiaries. This work may provide scientific knowledge that can be used by decision makers to develop management strategies, such as ecological compensation to mitigate damage from sandstorms in the study area.

Keywords: wind erosion prevention; ecosystem service flow; sandstorm; service-benefitting areas; service-providing areas

1. Introduction

Human welfare has received increasing attention in the study of ecosystem services, which are the ecosystem functions and processes that benefit humans [1–4]. To understand ecosystem services and their impacts on human welfare, many researchers have simultaneously investigated service demand and service supply [5–7]. Burkhard et al. [8] presented a conceptual framework linking ecosystems, ecosystem services, and human well-being as the supply and demand sides of human-environmental systems. Furthermore, there have been many studies of ecosystem service supply and demand and their balance [7–9]. However, the locations where services are provided and those where demand exists do not always match in these studies [10]. Wei et al. [11] noted that ecosystem service supply-demand mismatches strongly impact human well-being because they result in unsatisfied demand.

According to the studies of Costanza [12] and Fisher et al. [2], supply-demand mismatches exist for several types of ecosystem services, such as global non-proximal, directional and omnidirectional services, the supply-demand mismatches of which can be addressed by investigating their flow, especially for flow-dependent ecosystem services [13,14]. The spatial flow of ecosystem services reflects the spatial relationships between service-providing areas (SPAs) and the service-benefitting areas (SBAs), and defines the spatial ranges of these areas, which can be used to determine the spatial extent of the stakeholders involved in ecological payments and ecological compensation. Many studies of the flow of ecosystem services have been conducted [14–16], but most have addressed the conceptual framework of flows, while only a few have investigated the flow paths of specific services [17,18]. Turner et al. [19] investigated the ecosystem service flows of habitat protection, extracted the spatial relationships between the SPAs and SBAs, and the estimated the beneficiary population. Palomo et al. [20] presented a diagram of ecosystem service flows from SPAs to SBAs representing scientific knowledge that could be used to inform the management of the national parks of Spain, and Serna-Chavez et al. [21] developed an ecosystem service flow framework and introduced an indicator of the proportion of SBAs supported by spatial ecosystem service flows from SPAs as a measure of the spatial segregation between the two areas. More specifically, Bagstad et al. [13,22] developed a systematic approach to quantify ecosystem service flows and mapped the service supply, demand and flow of carbon sequestration and storage, riverine flood regulation, reservoir sediment regulation, open space proximity, and scenic viewsheds using the Artificial Intelligence for Ecosystem Services (ARIES) method. Finally, Li et al. [18] developed a freshwater ecosystem service flow model, which was similar to that of Bagstad et al., to investigate the flow of the service of water supply in Beijing-Tianjin-Hebei, China and emphasized the need to understand the connection between SPAs and SBAs.

Wind erosion is the wind-driven movement of soil particles, and it involves the entrainment, transport, and deposition of soil grains by air streams in arid and semi-arid regions around the world [23]. It is a serious environmental threat that leads to changes in global biochemical cycles, declines in agricultural productivity, damage to property, and hazards to human health, and it contributes to climate change. The total land area affected by wind erosion is 549 Mha, of which 296 Mha is severely affected [24]. Using Total Ozone Mapping Spectrometer (TOMS) data, Prospero et al. [25] determined that the largest and most persistent sources of atmospheric dust are in a broad "dust belt" that extends from the west coast of North Africa through the Middle East and central and southern Asia to China, where the dust-source regions are the Tarim Basin, the Gobi region, and the Hexi Corridor [26]. Wind erosion affects landform evolution, biogeochemical cycles, climate, air quality, primary productivity, soil fertility, infrastructure, buildings, human health, and transportation in downwind areas at both the local and regional scales [27–31], and its influencing factors primarily include climate warming and drying and human activities, such as grassland reclamation, overgrazing, furrow farming, mining, and infrastructure construction [27,32–34].

Wind erosion prevention is one of the most important services supplied by ecosystems in arid and semi-arid regions [35–37]. The vegetation in such ecosystems slows wind velocities, so increasing vegetation coverage results in greater soil retention. Zhao et al. [38] indicated that straw checkerboards and belts of sand-fixing plants could reduce wind speeds by 70% and found that the rate of sand transported to farmlands was reduced by 96% if the wind passed through an oasis-protection system. In a study by Pierre et al. [39], the horizontal mass flux for rangeland was less than that for cropland by a factor of approximately 1.5 because the millet began growing approximately 2–3 weeks later than the annual grass. Wind erosion prevention is a preventive ecosystem service that provides benefits by absorbing a detrimental carrier before it reaches users [13,40], and these benefits include reduced loss of soil nutrients, mitigation of atmospheric dust, decreased deflation hazards to infrastructure, fewer traffic accidents, and local or downwind reductions in negative health effects.

The path by which dust is transferred from a source area to a sink area is the flow path for wind erosion prevention. Several kinds of models have been used to simulate the process of dust transport including the Weather Research and Forecasting (WRF)-Chem, WRF-Dust, Global Environmental Multiscale (GEM)-AQ/EC, Community Atmosphere Model (CAM), Models-3/Community Multiscale Air Quality (CMAQ), and the Hybrid Single-Particle Lagrangian Integrated Trajectory (HYSPLIT) models [41–45]. The resolutions of the WRF-Chem, WRF-Dust, GEM-AQ/EC, CAM, and Models-3/CMAQ simulation results are relatively high, but the models require high-quality hardware and long run times as well as many input parameters. However, HYSPLIT, which can be obtained from the Air Research Laboratory (ARL) of the National Oceanic and Atmospheric Administration quickly and simply simulates the trajectories of dust-laden air with a horizontal resolution of 1.5° × 1.5° or 2.5° × 2.5° using National Centers for Environmental Prediction (NCEP) reanalysis data, and these trajectories can be used as the flow paths of the transported dust [46]. The HYSPLIT model is a complete system for computing simple air parcel trajectories and simulating complex transport, dispersion, chemical transformation, and deposition [45], and it has been widely used in simulations describing the atmospheric transport, dispersion, and deposition of pollutants and hazardous materials [47–50]. Tan et al. [51] simulated the trajectories of spring dust storms in Inner Mongolia of China with HYSPLIT and identified the impact areas, and Rashki et al. [52] similarly examined the trajectories of dust storm originating in the Sistan region of south-eastern Iran and the affected areas.

Hunshandake, which lies in Inner Mongolia of China, is one of the regions from which the sand and sandstorms in eastern Asia originate. Human activity has been found to be the dominant factor controlling the increase in desertification [53], so to ensure the benefit of wind erosion prevention, the people of Hunshandake should plant more vegetation, reduce the sizes of their herds, return their cropland to grassland, close their mines, and decrease the rates of industrialization and urbanization. However, these measures are disadvantageous to their way of life, so the associated losses should be reimbursed as the benefits of wind erosion prevention accrue to people in the downwind areas, as well as locally. Thus, it is crucial to identify the downwind areas based on the flow paths of the prevented wind erosion. In this study, we used HYSPLIT to simulate the flow paths of prevented wind erosion in terms of dust trajectories under the hypothesethat no vegetation coverage was present in the source area of the sand and then interpolated the trajectories to identify the benefit areas. The people living in these areas (the SBAs) could pay for the losses to the people in the SPAs to improve wind erosion prevention in Hunshandake, of Inner Mongolia.

2. Materials and Methods

2.1. Study Area

The key ecological function area (KEFA) for the protection of desertification in Hunshandake (which is centred on 43.09°N 114.79°E) is in the middle of Inner Mongolia and northern Hebei Province, China, and it covers an area of 160,000 km^2 (Figure 1). It is in the northern Yinshan Mountains and the eastern Mongolian Plateau with an average altitude of 1300 m. The area has an arid to semi-arid and temperate-continental monsoon climate that is characterized by short, warm, dry summers, and long, cold winters. The mean annual temperature is 0~3 °C; the annual precipitation is 350 mm; and, the annual evaporation is 1600 mm. The mean annual wind speed is 4~5 m/s, with maximum values of 24~28 m/s, and the number of days with wind speeds exceeding 17.2 m/s varies from 60 to 80. Furthermore, this area is in the agro-pastoral region of northern China, where the land cover types are primarily grassland and cropland (Figure 2), and it has suffered considerably from desertification due to increased livestock densities and cropland area since the 1980s. The driving factors of desertification include the warm and dry climate and human activity [54], but human activity has been identified as the dominant factor [53,55].

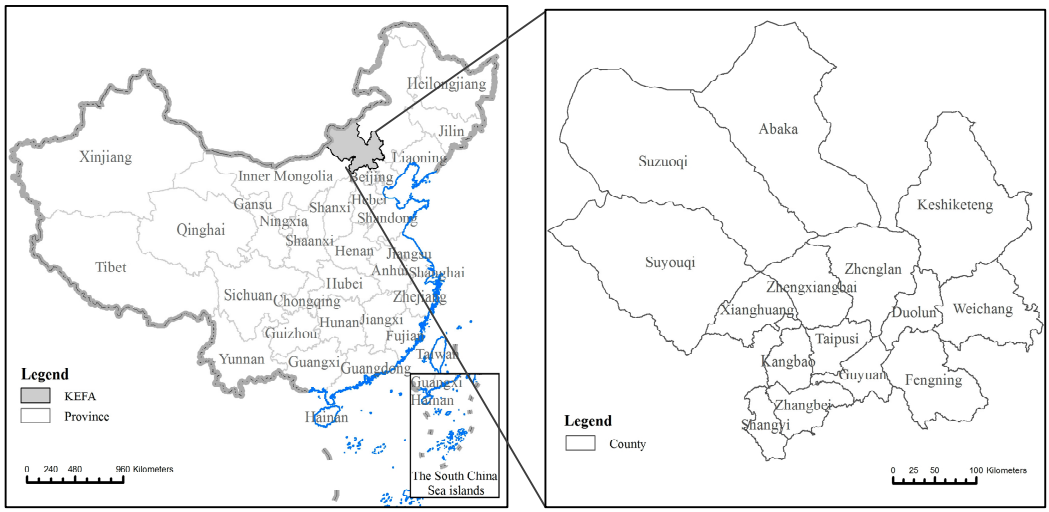

Figure 1. Location of the study area.

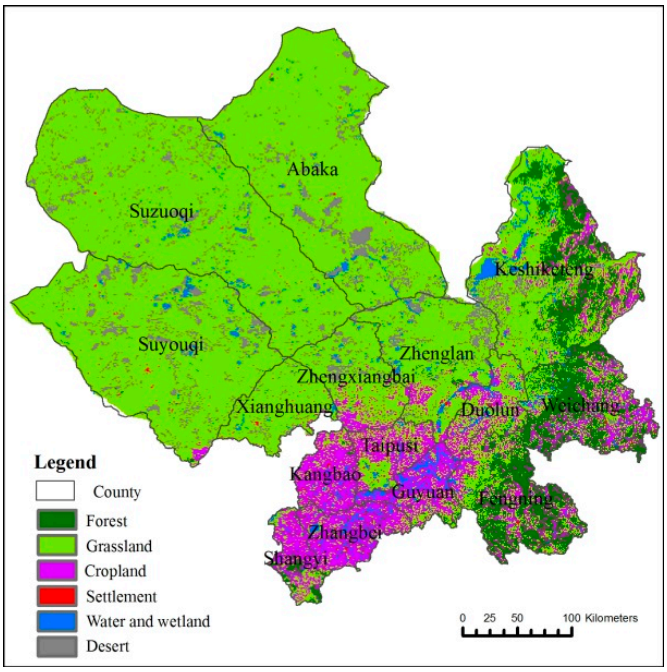

Figure 2. Land cover in the key ecological function area (KEFA) of Hunshandake.

2.2. Methods

2.2.1. Hypotheses Used to Simulate the Flow of Prevented Wind Erosion

The flow of the prevented wind erosion is the flow of the detrimental carrier, that is, dust, from its source area when the wind speed is equal to or greater than a threshold. We examined the flow under three hypotheses: first, no vegetation cover or other barriers to sand transport existed; that is, there were sufficient sand sources; second, the sand particles were easily blown when the wind speed was greater than or equal to the threshold; and third, the second hypotheses occurred along with air conditions that were strongly thermally unstable, so the blown sand could be transferred with the air masses to downwind areas and deposited along the air mass trajectories. In this case, the trajectories of the air masses would determine the paths of the prevented wind erosion and the benefit areas, which could be simulated with HYSPLIT.

2.2.2. Simulation of the Flow Paths of the Prevented Wind Erosion

In this study, forward-trajectory analysis was used to determine the flow paths of the prevented wind erosion [52]. The 5-day forward trajectories, which had starting elevations of 500 m above ground level and were centred on the 43.09°N 114.79°E pixel (i.e., Hunshandake) were simulated with HYSPLIT every 6 h from 0:00 on 1 January to 24:00 on 31 December in 2010. Meteorological data from the NCEP/National Center for Atmospheric Research (NCAR) reanalysis (which are available from 1948 to the present) were used for the trajectory simulations, and trajectories were only simulated when the maximum 10-min average wind speed in 1 h was greater than, or equal to, the threshold wind speed. The average threshold wind speed for sand without vegetation cover in Hunshandake is 5.5 m/s [56].

2.2.3. Identifying the Benefit Areas of the Prevented Wind Erosion

The hazards produced by sandstorms along the trajectories include erosion by strong wind and sand flow, sand deposition, and air pollution, so wind erosion prevention by vegetation reduces the hazards associated with sandstorms and produces benefits for people living along the trajectories. These benefits include reduced damage to farming, animal husbandry, forestry production, infrastructure, and health, as well as the prevention of reduced visibility, and the areas where these benefits are realized include forest, grassland, cropland, settlements, and wetland (Figure 3). The 2010 land cover data were provided by the Institute of Remote Sensing and Digital Earth of the Chinese Academy of Sciences [57], and the benefit areas were identified using the simulated trajectories of the prevented wind erosion [13,58]. The trajectories were interpolated onto a $1^\circ \times 1^\circ$ grid with HYSPLIT to obtain the benefit extent, and the value assigned to each grid cell was the frequency with which the trajectories passed through the cell, which was calculated as follows:

$$p_i = \frac{L_i}{L} \quad (1)$$

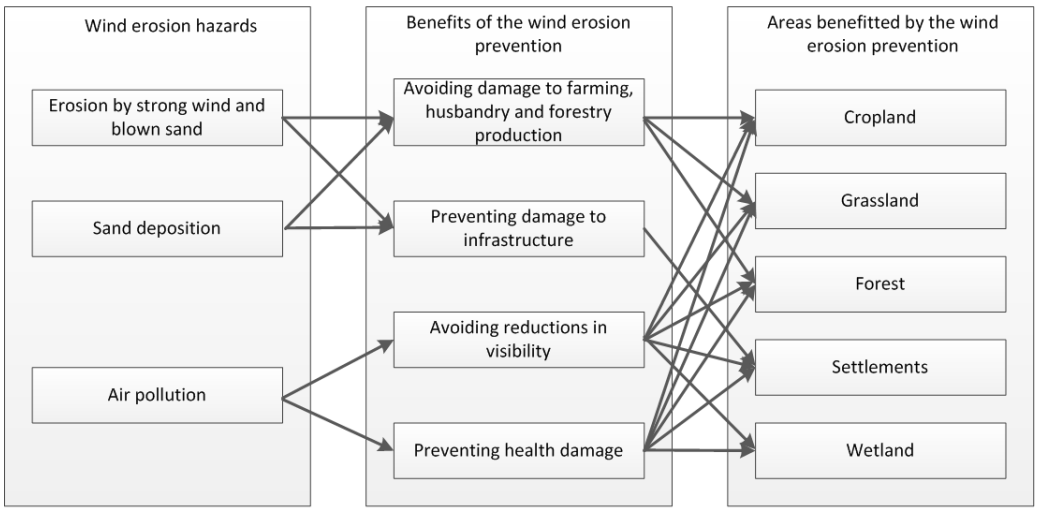

Figure 3. Framework used to identify the benefit areas of wind erosion prevention. As a preventive service, wind erosion prevention provides benefits by limiting the flow of a detrimental carrier (dust) to vulnerable human populations, for which the hazards include (1) erosion by strong wind and blown sand, (2) sand deposition, and (3) air pollution. Therefore, the benefits of the prevented wind erosion service are (1) the avoidance of damage to farming, husbandry and forestry production; (2) the prevention of damage to infrastructure; (3) the avoidance of reduced visibility, and (4) the prevention of negative health impacts. The benefit areas are the places where the preventive benefits occur including (1) cropland, (2) grassland, (3) forest, (4) settlements, and (5) wetland.

Here, p_i is the frequency with which the trajectories passed through grid cell i; L_i is the number of trajectories that passed through grid cell i; and L is the total number of trajectories from the starting point.

The frequency with which the trajectories passed through a grid cell were treated as a proxy for the benefit of wind erosion prevention that accrued to the people in the cell. Grid cells with higher values imply that the people in those cells received greater benefits from the prevention of wind erosion by the ecosystems in the KEFA of Hunshandake than the people in other grid cells, and the benefits included reduced damage to farming, animal husbandry, forestry production, infrastructure, and health, as well as the prevention of reduced visibility (Figure 3). The benefitting population was identified from the population distribution data and the grid cells through which the simulated trajectories passed, and the Gross Domestic Product (GDP) of these cells increased because of the reduced damage to farming, animal husbandry, and forestry production due to the prevention of wind erosion. The benefitting GDP was also identified using the GDP distribution data and the benefit extent. Population and GDP data for 2010 were provided by the Data Centre for Resources and Environmental Sciences (RESDC) of the Chinese Academy of Sciences (http://www.resdc.cn).

3. Results

3.1. Flow Paths of the Prevented Wind Erosion

In 2010, there were 1440 6-hourly wind speed records. The maximum wind speed was 14.4 m/s, the minimum 0 m/s, and the mean was 7.4 m/s. Approximately 465 of the wind speed records were greater than or equal to the threshold wind speed ($\geq$5.5 m/s). The number of times that the winds were $\geq$5.5 m/s was slightly greater in March, April, and May than those in the other months, whereas the corresponding values in February, June, and October were less than those in the other months (Figure 4).

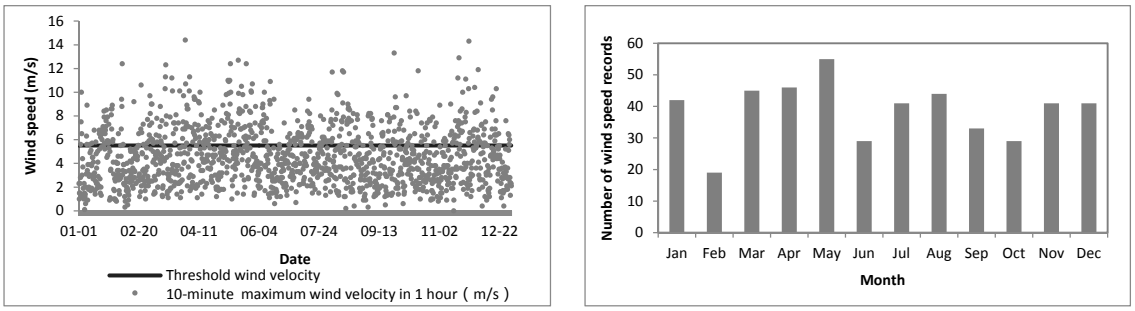

(**a**) (**b**)

Figure 4. Wind speed (**a**) and number of wind speed records in each month that equalled or exceeded the threshold wind speed (**b**) in the KEFA of Hunshandake in 2010.

The simulated dust storm trajectories and the flow paths of the prevented wind erosion of the KEFA of Hunshandake mainly passed through China, North Korea, South Korea, Japan, Mongolia, and Russia (Figure 5a). Thus, the benefits of the prevented wind erosion accrued to other countries than China.

Wind erosion was prevented along 465 flow paths, of which 146 occurred in spring (from March to May), 114 in summer (from June to August), 103 in autumn (from September to November), and 102 in winter (from December to February). The number of such flow paths was much greater in spring than those in the other seasons, and the patterns of the flow paths also varied among the seasons. In spring, most of the flow paths extended to the northeast of the KEFA, and a few extended to the southeast. The prevented wind erosion benefits mainly extended to the northeast in summer. The patterns of the flow paths were similar in autumn and winter and extended to the east and south (Figure 5b to

Figure 5e). The orientations of these paths resulted from the interaction between cold air from Siberia, which prevails from October to April of the next year, and warm air from the East Asian monsoon, which is stronger from May to September [59–61].

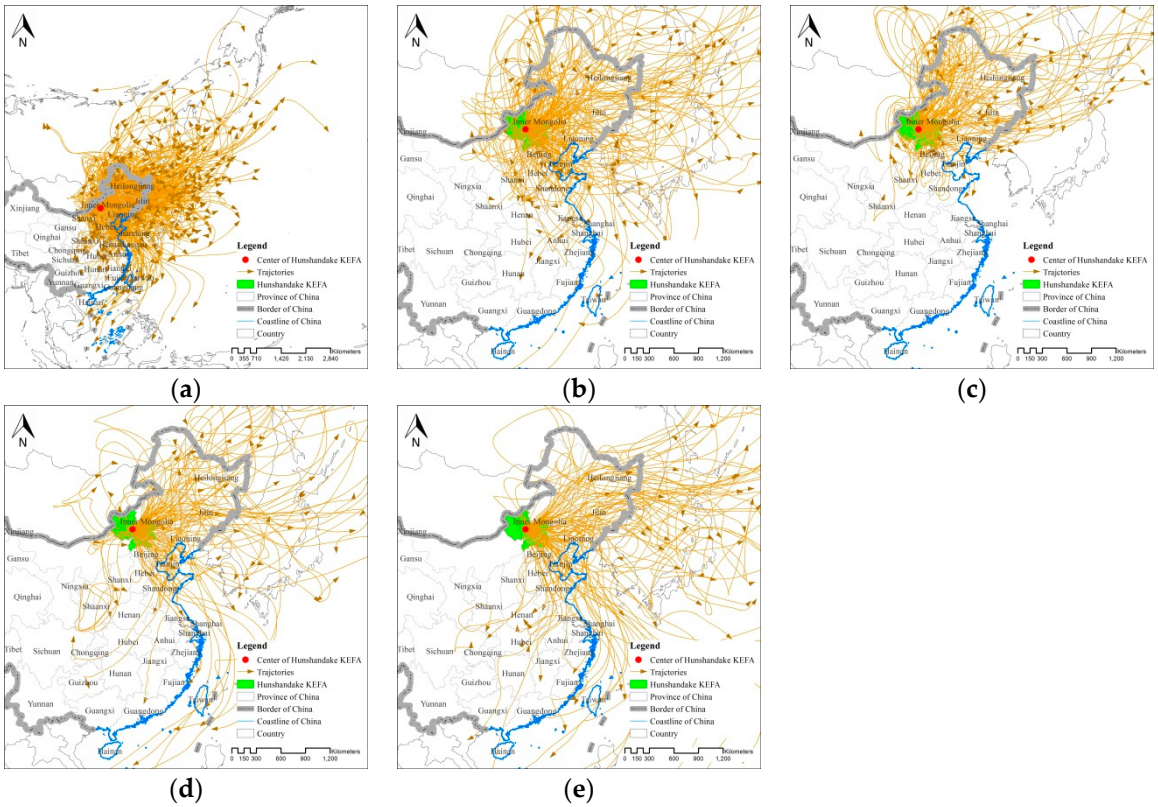

Figure 5. Flow paths of the wind erosion prevented by the ecosystems in the KEFA of Hunshandake. The flow paths represent the trajectories of dust simulated by Hybrid Single-Particle Lagrangian Integrated Trajectory (HYSPLIT) when the wind speeds were ≥5.5 m/s, and they extended over a large area (**a**). We classified the flow paths in China into four categories: those occurring during spring (**b**), summer (**c**), autumn (**d**) and winter (**e**).

3.2. *Benefit Areas of the Prevented Wind Erosion*

In China, the area that benefitted from the prevention of wind erosion by the ecosystems in the KEFA of Hunshandake was mostly in the eastern part of the country, and it was estimated to be 3.78×10^6 km^2, which represents 39.21% of the total area of China. The grid cells through which many (≥10%) of the trajectories passed were mainly in the western part of north-eastern China and the eastern part of northern China, such as eastern Inner Mongolia, Hebei Province and the municipality of Beijing, western Liaoning Province, and Jilin Province (Figure 6a). This result implies that these grid cells received much greater benefits from the wind erosion prevented by the ecosystems in the KEFA of Hunshandake than the other grid cells. As the distance from the KEFA of Hunshandake increased, the benefits accrued to each grid cell tended to gradually decrease. Overall, the grid cells in the southern part of the benefit areas received less benefit than those in the northern part, but the benefitting areas in China varied seasonally. The number of benefitting grid cells was smallest in summer, and most were in north-eastern China and northern China. In spring, the benefitting grid cells extended southward and included eastern China. In autumn and winter, these areas progressively expanded to the southwest, but the eastern part of western China and southern China were also affected (Figure 6b to Figure 6e).

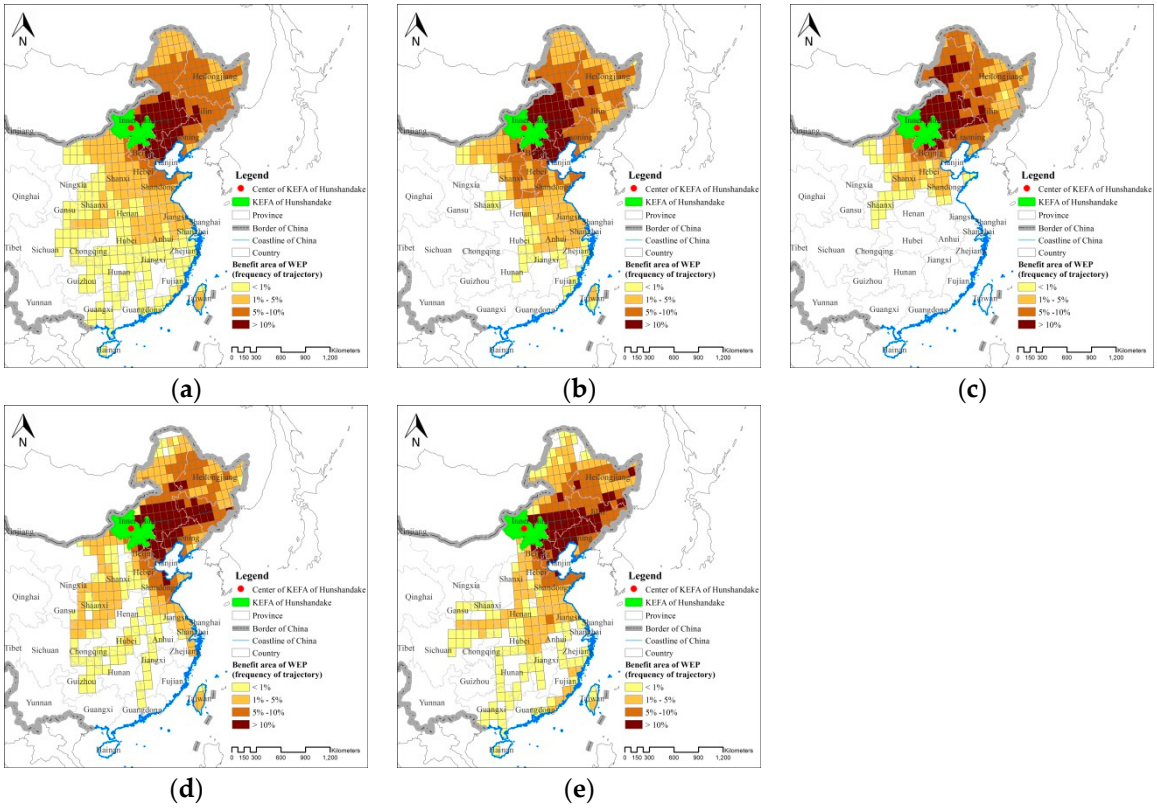

Figure 6. Areas in China benefitting from the wind erosion prevented by the ecosystems in the KEFA of Hunshandake in 2010 (**a**) and their patterns in different seasons (**b**: spring, **c**: summer, **d**: autumn and **e**: winter). The value of each grid cell is the ratio of the number of simulated trajectories passing through the grid cell to the total number of simulated trajectories. These values represent the benefit of wind erosion prevention that accrued to the people in each grid cell; higher values (shown in darker colours) imply that the people living in those grid cells derived greater benefits.

3.3. Benefitting Land Cover Type, Population and GDP Associated with the Prevented Wind Erosion

The area that benefited from the prevention of wind erosion by the KEFA of Hunshandake was approximately 3.67×10^6 km^2, of which 35.86% was cropland, 33.82% forest, 17.41% grassland, 5.27% wetland, and 4.82% settlements (Table 1), and it accounted for 48.40% of the total area of cropland, forest, grassland, wetland, and settlements in China. The benefitting croplands were mainly in the Sanjiang Plain of Helongjiang Province, the northern China Plain of Beijing, and the provinces of Hebei, Shandong, Henan, Anhui and Jiangsu. The benefitting settlements included the cities of Beijing, Tianjin, Jinan, Zhengzhou, Nanjing, and Shanghai, as well as many rural settlements dispersed within cropland (Figure 7a). The benefitting population was estimated to be 1.00×10^9 people, corresponding to 74.51% of the total population of China in 2010 (Table 2), and it was mostly distributed in the Beijing-Tianjin-Hebei metropolitan area, the hinterland of the northern China Plain, the Yangtze River Delta metropolitan area, and the eastern part of the Sichuan Basin (Figure 7b). The benefit to GDP from the prevention of wind erosion was 27.72×10^{12} RMB, which corresponds to 67.11% of the total GDP of China in 2010 (Table 2), and it mainly occurred in the Beijing-Tianjin-Hebei metropolitan area, the Yangtze River Delta metropolitan area, eastern Liaoning Peninsula, and the middle of the northern China Plain (Figure 7c). As the eastern part of China is much more highly populated and developed than the western part, the proportions of the benefit for population and GDP were much higher than those for land cover.

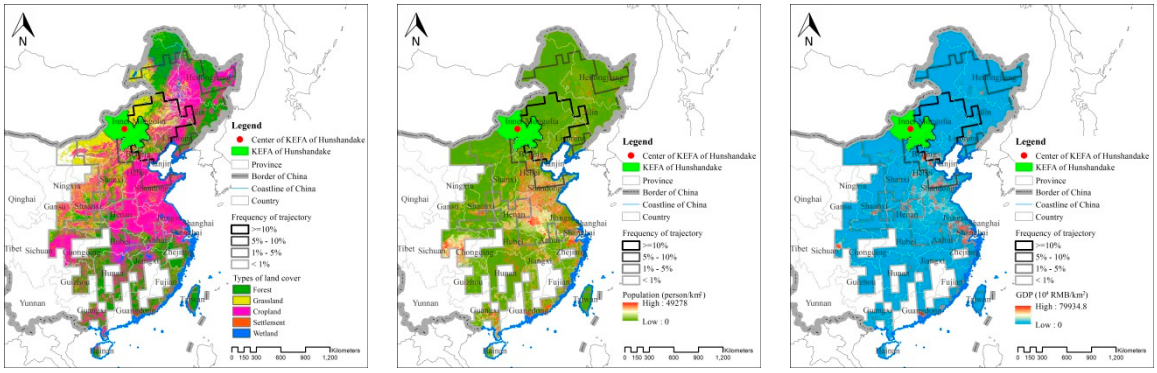

(**a**) (**b**) (**c**)

Figure 7. Benefitting land cover (**a**), population (**b**), and GDP (**c**) in China from the wind erosion prevented by the KEFA of Hunshandake in 2010.

Table 1. Land cover benefits from the wind erosion prevented by the KEFA of Hunshandake.

Frequency of Trajectory	Benefitting Land Cover (10^3 km^2)					
	Forest	Grassland	Cropland	Settlement	Wetland	In Sum
<1%	591.91	187.10	480.69	55.26	49.08	1364.04
1~5%	359.04	240.87	462.80	74.18	74.40	1211.29
5~10%	250.39	120.90	299.38	38.19	60.51	769.37
≥10%	76.20	108.76	111.74	14.43	15.06	326.18
In sum	1277.54	657.64	1354.61	182.05	199.04	3670.88

Table 2. Population and GDP benefits from the wind erosion prevented by the KEFA of Hunshandake.

Frequency of Trajectory	Benefitting Area (10^6 km^2)	Ratio to the Total Area of China (%)	Benefitting Population (10^6 people)	Ratio to the Total Population of China (%)	Benefitting GDP (10^{12} RMB)	Ratio to the Total GDP of China (%)
<1%	1.42	14.71	453.19	33.80	11.02	26.68
1~5%	1.23	12.76	355.77	26.53	9.80	23.72
5~10%	0.78	8.14	141.11	10.52	5.38	13.02
≥10%	0.35	3.60	49.09	3.66	1.52	3.69
In sum	3.78	39.21	999.17	74.51	27.72	67.11
China	9.63	100	1340.91	100	41.30	100

4. Discussion

4.1. Spatial Relationship between Service Providing Areas (SPAs) and Service Benefitting Areas (SBAs)

The study of ecosystem services is anthropocentric and utilitarian, and the values of the services provided by ecosystems depend on the utility that people derive from their consumption, either directly or indirectly [62]. Therefore, investigations into the provision of, and demand for, ecosystem services help reveal the utility that people obtain from these services. Burkhard et al. [8] presented a conceptual framework linking ecosystems and ecosystem services and human well-being as the supply and demand sides, respectively, of human-environmental systems, and they also argued that ecosystem service supply and demand is closely related to proximity. Kroll et al. [6] investigated the supply and demand of the ecosystem services of energy, food, and water provision along the rural-urban gradient of the Leipzig-Halle region of eastern Germany using spatially explicit methods, and Larondelle and Lauf [9] examined the supply and demand of five urban ecosystem services and their balances at the block, neighbourhood, and whole-city scales in Berlin, Germany. However, the budgets or balances between supply and demand, as identified in these studies, failed to reflect the actual situation because no spatial relationship was found between the SPAs and SBAs. Several other researchers have identified mismatches between SPAs and SBAs [10,63–65] that include cases in which

the water provided by a study area is used by the people in the downstream areas while the people within the study area use water from farther upstream. Therefore, it is difficult to develop effective management policies based on the results of such supply and demand budgets, so several studies have investigated the flow of ecosystem services to determine the spatial relationships between SPAs and SBAs [14,66,67]. However, few studies have investigated the flow of wind erosion prevention. In this study, we determined the spatial connections between SPAs and SBAs by simulating the flow path of prevented wind erosion, and the trajectories of simulated sandstorms were used to identify the SBAs under the hypothesis of no vegetation cover in the study area. The benefitting population and GDP were also assessed within the SBAs, and we developed a rational relationship between the SPAs and SBAs and identified the actual beneficiaries. The results of this study represent scientific knowledge that can be used by decision makers to develop sandstorm mitigation strategies.

4.2. Implications for Eco-Compensation

Human activities, such as reclamation and planting, overgrazing, and mining, are thought to be important drivers of desertification in the KEFA of Hunshandake [53], and they have increased desertification and reduced vegetation coverage, which has caused this area to become an additional source of sand. If the wind speed equals or exceeds the threshold value, the sand is easily transferred downwind by the air mass, so it is necessary to adopt measures to limit or change human activities to mitigate the downwind impacts of sandstorms. These measures include reducing reclamation, limiting the intensity of grazing and mining, and rehabilitating vegetation. However, most of these measures would result in economic losses and be disadvantageous to the short-term welfare of the local people, but eco-compensation could help to compensate for these losses. Currently, the government provides an insufficient KEFA transfer payment [68], but ecological payments from people in the downwind areas in exchange for the prevention of wind erosion by the ecosystems in the KEFA of Hunshandake would make up the difference. If the total payment were to be determined, the results of this study could be used to identify the area over which people should pay, and allocate the amount based on the frequency at which the simulated trajectories pass through each grid cell. The funds from the ecological payment could be directly used to encourage the local people of Hunshandake to adopt measures to mitigate sandstorms such as reducing livestock numbers, limiting mining, returning cropland to grassland or forest, sowing grass, planting trees, and constructing physical sand barriers.

4.3. Limitations

However, some uncertainties and limitations of this method need to be considered. (1) The simulation of sandstorms was simplified in our study. Sandstorms were assumed to occur if the wind speed equalled or exceeded the wind speed threshold, and sufficient sand sources without vegetation cover were assumed to exist. However, we did not account for atmospheric instability in this study, and sandstorms actually occur when three conditions are met: a sufficient sand source, strong wind, and atmospheric instability. In the future, these three conditions should be incorporated when simulating the flow of wind erosion prevention; (2) We did not exclude the trajectories that corresponded to actual sandstorms because we assumed that the vegetation in the study area mitigated the impacts on the people in the downwind areas; (3) Based on the available data, we simulated the trajectories of the air masses at the centre of the KEFA of Hunshandake using the wind speed data from the nearest weather station, and the trajectories from the centre of the study area were used to represent the flow paths of the prevented wind erosion over the whole study area without considering the spatial heterogeneity of the meteorological data, which may have affected the accuracy of the results. In the future, the appropriate study area scale for simulating sandstorm trajectories with these meteorological data should be considered. Furthermore, more sophisticated models incorporating existing wind erosion models and sand deposition simulation models should be developed to quantify the flow of wind erosion prevention from the SPAs to the SBAs.

5. Conclusions

Researching the flow of ecosystem services is essential for determining actual SBAs, as well as the spatial relationships between SPAs and SBAs. In this study, we simulated the flow paths of the wind erosion prevented by the ecosystems in the KEFA of Hunshandake and identified the SBAs and the land cover, population, and GDP benefits. Furthermore, we proposed relationships between the SPAs and the SBAs as well as a proxy for the benefits realized by the SBAs. From this research, we conclude that wind erosion was prevented along 465 flow paths in 2010, and these flow paths mostly extended to the eastern part of the study area. The SBAs were estimated to cover 39.21% of the total area of China, and the grid cells through which many ($\geq$10%) of the trajectories passed were mainly located in the western part of north-eastern China and the eastern part of northern China. The benefitting population and GDP accounted for 74.51% of the total population and 67.11% of the total GDP of China in 2010. The results represent scientific knowledge that can be used to make decisions about ecological payments to promote the mitigation of sandstorms in the KEFA of Hunshandake. Our approach focuses on the spatial flow of wind erosion prevention and can be further applied to other locations to identify the benefitting areas and the relative benefits. Future studies are needed to accurately determine the sand transported from SPAs and deposited in SBAs when simulating the flow of the ecosystem service of wind erosion prevention.

Acknowledgments: This study was sponsored by the National Natural Science Foundation of China (31400411) and the National Key Research & Development Program of China (2016YFC0503706 and 2016YFC0503403).

Author Contributions: Yu Xiao and Gaodi Xie co-designed the research. Yu Xiao analysed the data and wrote the paper. Lin Zhen revised the manuscript. Chunxia Lu and Jie Xu collected the data.

Conflicts of Interest: The authors declare no conflicts of interest.

References

1. De Groot, R.S.; Alkemade, R.; Braat, L.; Hein, L.; Willemen, L. Challenges in integrating the concept of ecosystem services and values in landscape planning, management and decision making. *Ecol. Complex.* **2010**, *7*, 260–272. [CrossRef]
2. Fisher, B.; Turner, R.K.; Morling, P. Defining and classifying ecosystem services for decision making. *Ecol. Econ.* **2009**, *68*, 643–653. [CrossRef]
3. Burkhard, B.; de Groot, R.; Costanza, R.; Seppelt, R.; Jørgensen, S.E.; Potschin, M. Solutions for sustaining natural capital and ecosystem services. *Ecol. Indic.* **2012**, *21*, 1–6. [CrossRef]
4. Xiao, Y.; Xie, G.; Lu, C.; Xu, J. Involvement of ecosystem service flows in human wellbeing based on the relationship between supply and demand. *Acta Ecol. Sin.* **2016**, *36*, 3096–3102, (In Chinese with English Summary).
5. Beier, C.; Patterson, T.; Chapin, F.S., III. Ecosystem Services and Emergent Vulnerability in Managed Ecosystems: A Geospatial Decision-Support Tool. *Ecosystems* **2008**, *11*, 923–938. [CrossRef]
6. Kroll, F.; Müller, F.; Haase, D.; Fohrer, N. Rural–urban gradient analysis of ecosystem services supply and demand dynamics. *Land Use Policy* **2012**, *29*, 521–535. [CrossRef]
7. Nedkov, S.; Burkhard, B. Flood regulating ecosystem services—Mapping supply and demand, in the Etropole municipality, Bulgaria. *Ecol. Indic.* **2012**, *21*, 67–79. [CrossRef]
8. Burkhard, B.; Kroll, F.; Nedkov, S.; Müller, F. Mapping ecosystem service supply, demand and budgets. *Ecol. Indic.* **2012**, *21*, 17–29. [CrossRef]
9. Larondelle, N.; Lauf, S. Balancing demand and supply of multiple urban ecosystem services on different spatial scales. *Ecosyst. Serv.* **2016**, *22*, 18–31. [CrossRef]
10. Brauman, K.A.; Daily, G.C.; Duarte, T.K.; Mooney, H.A. The nature and value of ecosystem services: An overview highlighting hydrologic services. *Annu. Rev. Environ. Resour.* **2007**, *32*, 67–98. [CrossRef]
11. Wei, H.; Fan, W.; Wang, X.; Lu, N.; Dong, X.; Zhao, Y.; Ya, X.; Zhao, Y. Integrating supply and social demand in ecosystem services assessment: A review. *Ecosyst. Serv.* **2017**, *25*, 15–27. [CrossRef]
12. Costanza, R. Ecosystem services: Multiple classification systems are needed. *Biol. Conserv.* **2008**, *141*, 350–352. [CrossRef]

13. Bagstad, K.J.; Johnson, G.W.; Voigt, B.; Villa, F. Spatial dynamics of ecosystem service flows: A comprehensive approach to quantifying actual services. *Ecosyst. Serv.* **2013**, *4*, 117–125. [CrossRef]
14. Goldenberg, R.; Kalantari, Z.; Cvetkovic, V.; Mörtberg, U.; Deal, B.; Destouni, G. Distinction, quantification and mapping of potential and realized supply-demand of flow-dependent ecosystem services. *Sci. Total Environ.* **2017**, *593–594*, 599–609. [CrossRef] [PubMed]
15. Owuor, M.A.; Icely, J.; Newton, A.; Nyunja, J.; Otieno, P.; Tuda, A.O.; Oduor, N. Mapping of ecosystem services flow in Mida Creek, Kenya. *Ocean Coast. Manag.* **2017**, *140*, 11–21. [CrossRef]
16. Vrebos, D.; Staes, J.; Vandenbroucke, T.; D'Haeyer, T.; Johnston, R.; Muhumuza, M.; Kasabeke, C.; Meire, P. Mapping ecosystem service flows with land cover scoring maps for data-scarce regions. *Ecosyst. Serv.* **2015**, *13*, 28–40. [CrossRef]
17. Xiao, Y.; Zhang, C.; Xu, J. Areas benefiting from water conservation in key ecological function areas in China. *J. Resour. Ecol.* **2015**, *6*, 375–385.
18. Li, D.; Wu, S.; Liu, L.; Liang, Z.; Li, S. Evaluating regional water security through a freshwater ecosystem service flow model: A case study in Beijing-Tianjian-Hebei region, China. *Ecol. Indic.* **2017**, *81*, 159–170. [CrossRef]
19. Turner, W.R.; Brandon, K.; Brooks, T.M.; Gascon, C.; Gibbs, H.K.; Lawrence, K.S.; Mittermeier, R.A.; Selig, E.R. Global biodiversity conservation and the alleviation of poverty. *Bioscience* **2012**, *62*, 85–92. [CrossRef]
20. Palomo, I.; Martín-López, B.; Potschin, M.; Haines-Young, R.; Montes, C. National Parks, buffer zones and surrounding lands: Mapping ecosystem service flows. *Ecosyst. Serv.* **2013**, *4*, 104–116. [CrossRef]
21. Serna-Chavez, H.M.; Schulp, C.J.E.; van Bodegom, P.M.; Bouten, W.; Verburg, P.H.; Davidson, M.D. A quantitative framework for assessing spatial flows of ecosystem services. *Ecol. Indic.* **2014**, *39*, 24–33. [CrossRef]
22. Bagstad, K.J.; Villa, F.; Batker, D.; Harrison-Cox, J.; Voigt, B.; Johnson, G.W. From theoretical to actual ecosystem services: Mapping beneficiaries and spatial flows in ecosystem service assessments. *Ecol. Soc.* **2014**, *19*, 64. [CrossRef]
23. Ravi, S.; Zobeck, T.M.; Over, T.M.; Okin, G.S.; D'Odorico, P. On the effect of moisture bonding forces in air-dry soils on threshold friction velocity of wind erosion. *Sedimentology* **2006**, *53*, 597–609. [CrossRef]
24. Lal, R. Soil erosion and the global carbon budget. *Environ. Int.* **2003**, *29*, 437–450. [CrossRef]
25. Prospero, J.M.; Ginoux, P.; Torres, O.; Nicholson, S.E.; Gill, T.E. Environmental characterization of global sources of atmospheric soil dust identified with the nimbus 7 total ozone mapping spectrometer (TOMS) absorbing aerosol product. *Rev. Geophys.* **2002**, *40*, 2-1–2-31. [CrossRef]
26. Shao, Y.; Dong, C.H. A review on East Asian dust storm climate, modelling and monitoring. *Glob. Planet. Chang.* **2006**, *52*, 1–22. [CrossRef]
27. Ravi, S.; D'Odorico, P.; Breshears, D.D.; Field, J.P.; Goudie, A.S.; Huxman, T.E.; Li, J.; Okin, G.S.; Swap, R.J.; Thomas, A.D.; et al. Aeolian processes and the biosphere. *Rev. Geophys.* **2011**. [CrossRef]
28. Baddock, M.C.; Strong, C.L.; Murray, P.S.; McTainsh, G.H. Aeolian dust as a transport hazard. *Atmos. Environ.* **2013**, *71*, 7–14. [CrossRef]
29. Yan, Y.; Sun, Y.; Ma, L.; Long, X. A multidisciplinary approach to trace Asian dust storms from source to sink. *Atmos. Environ.* **2015**, *105*, 43–52. [CrossRef]
30. Hoffmann, C.; Funk, R.; Reiche, M.; Li, Y. Assessment of extreme wind erosion and its impacts in Inner Mongolia, China. *Aeolian Res.* **2011**, *3*, 343–351. [CrossRef]
31. Sharratt, B.S.; Lauer, D. Particulate matter concentration and air quality affected by windblown dust in the Columbia Plateau. *J. Environ. Qual.* **2006**, *35*, 2011–2016. [CrossRef] [PubMed]
32. Wang, T.; Wu, W.; Zhao, H.; Hu, M.; Zhao, A. Analyses on Driving Factors to Sandy Desertification Process in Horqin Region. *J. Desert Res.* **2004**, *24*, 519–528.
33. Wang, X.M.; Li, J.J.; Dong, G.R.; Xia, D.S. Aeolian climate evolvement and the response of disertification in the sand region of Northern China in the past 50 years. *Chin. Sci. Bull.* **2007**, *52*, 2882–2888.
34. Shao, Y.P. *Physics and Modelling of Wind Erosion*; Springer: Dordrecht, The Netherlands, 2008.
35. Syrbe, R.-U.; Walz, U. Spatial indicators for the assessment of ecosystem services: Providing, benefiting and connecting areas and landscape metrics. *Ecol. Indic.* **2012**, *21*, 80–88. [CrossRef]
36. Borrelli, P.; Lugato, E.; Montanarella, L.; Panagos, P. A New Assessment of Soil Loss Due to Wind Erosion in European Agricultural Soils Using a Quantitative Spatially Distributed Modelling Approach. *Land Degrad. Dev.* **2017**, *28*, 335–344. [CrossRef]

37. Halim, A.; Normaniza, O. The effects of plant density of Melastoma malabathricum on the erosion rate of slope soil at different slope orientations. *Int. J. Sediment Res.* **2015**, *30*, 131–141. [CrossRef]
38. Zhao, W.; Hu, G.; Zhang, Z.; He, Z. Shielding effect of oasis-protection systems composed of various forms of wind break on sand fixation in an arid region: A case study in the Hexi Corridor, northwest China. *Ecol. Eng.* **2008**, *33*, 119–125. [CrossRef]
39. Pierre, C.; Kergoat, L.; Bergametti, G.; Mougin, É.; Baron, C.; Abdourhamane Toure, A.; Rajot, J.-L.; Hiernaux, P.; Marticorena, B.; Delon, C. Modeling vegetation and wind erosion from a millet field and from a rangeland: Two Sahelian case studies. *Aeolian Res.* **2015**, *19*, 97–111. [CrossRef]
40. Li, G.S.; Qu, J.J.; Han, Q.J.; Fang, H.Y.; Wang, W.F. Responses of three typical plants to wind erosion in the shrub belts atop Mogao Grottoes, China. *Ecol. Eng.* **2013**, *57*, 293–296. [CrossRef]
41. Grell, G.A.; Peckham, S.E.; Schmitz, R.; Mckeen, S.A.; Frost, G.; Skamarock, W.C.; Eder, B. Fully coupled "online" chemistry within the WRF model. *Atmos. Environ.* **2005**, *39*, 6957–6975. [CrossRef]
42. Ginoux, P.; Chin, M.; Tegen, I.; Prospero, J.M.; Holben, B.; Dubovik, O.; Lin, S.J. Sources and distributions of dust aerosols simulated with the GOCART model. *J. Geophys. Res. Atmos.* **2001**, *106*, 20255–20273. [CrossRef]
43. Gong, S.L.; Lavoué, D.; Zhao, T.L.; Huang, P.; Kaminski, J.W. GEM-AQ/EC, an on-line global multi-scale chemical weather modelling system: Model development and evaluation of global aerosol climatology. *Atmos. Chem. Phys.* **2012**, *12*, 8237–8256. [CrossRef]
44. Dennis, R.L.; Byun, D.W.; Novak, J.H.; Galluppi, K.J.; Coats, C.J.; Vouk, M.A. The next generation of integrated air quality modeling: EPA's models-3. *Atmos. Environ.* **1996**, *30*, 1925–1938. [CrossRef]
45. Stein, A.F.; Draxler, R.R.; Rolph, G.D.; Stunder, B.J.B.; Cohen, M.D.; Ngan, F. NOAA's HYSPLIT Atmospheric Transport and Dispersion Modeling System. *Bull. Am. Meteorol. Soc.* **2015**, *96*, 2059–2077. [CrossRef]
46. Wang, Y.; Stein, A.F.; Draxler, R.R.; de la Rosa, J.D.; Zhang, X. Global sand and dust storms in 2008: Observation and HYSPLIT model verification. *Atmos. Environ.* **2011**, *45*, 6368–6381. [CrossRef]
47. Li, W.; Wang, C.; Wang, H.; Chen, J.; Yuan, C.; Li, T.; Wang, W.; Shen, H.; Huang, Y.; Wang, R. Distribution of atmospheric particulate matter (PM) in rural field, rural village and urban areas of northern China. *Environ. Pollut.* **2014**, *185*, 134–140. [CrossRef] [PubMed]
48. Varga, G.; Újvári, G.; Kovács, J. Spatiotemporal patterns of Saharan dust outbreaks in the Mediterranean Basin. *Aeolian Res.* **2014**, *15*, 151–160. [CrossRef]
49. Engling, G.; He, J.; Betha, R.; Balasubramanian, R. Assessing the regional impact of Indonesian biomass burning emissions based on organic molecular tracers and chemical mass balance modeling. *Atmos. Chem. Phys.* **2014**, *14*, 8043–8054. [CrossRef]
50. Lv, B.; Zhang, B.; Bai, Y. A systematic analysis of $PM_{2.5}$ in Beijing and its sources from 2000 to 2012. *Atmos. Environ.* **2015**, *124*, 98–108. [CrossRef]
51. Tan, S.C.; Shi, G.Y.; Wang, H. Long-range transport of spring dust storms in Inner Mongolia and impact on the China seas. *Atmos. Environ.* **2012**, *46*, 299–308. [CrossRef]
52. Rashki, A.; Kaskaoutis, D.G.; Francois, P.; Kosmopoulos, P.G.; Legrand, M. Dust-storm dynamics over Sistan region, Iran: Seasonality, transport characteristics and affected areas. *Aeolian Res.* **2015**, *16*, 35–48. [CrossRef]
53. Xu, D.; Li, C.; Song, X.; Ren, H. The dynamics of desertification in the farming-pastoral region of North China over the past 10 years and their relationship to climate change and human activity. *CATENA* **2014**, *123*, 11–22. [CrossRef]
54. Li, H.W.; Yang, X.P. Advances and problems in the understanding of desertification in the Hunshandake Sandy Land during the last 30 years. *Adv. Earth Sci.* **2010**, *25*, 647–655.
55. Zheng, Y.R.; Xie, Z.X.; Robert, C.; Jiang, L.H.; Shimizu, H. Did climate drive ecosystem change and induce desertification in Otindag sandy land, China over the past 40 years? *J. Arid Environ.* **2006**, *64*, 523–541. [CrossRef]
56. He, J.; Wu, X.H.; Yang, T.T.; Li, P. Research on sand-fixing function of grassland based on threshold wind velocity. *Chin. J. Grassl.* **2013**, *35*, 103–107, (In Chinese with English Summary).
57. Zhang, Z.X.; Wang, X.; Wang, C.Y.; Zuo, L.J.; Wen, Q.K.; Dong, T.T.; Zhao, X.L.; Lu, B.; Yi, L. National land cover mapping by remote sensing under the control of interperted data. *J. Geo-Inf. Sci.* **2009**, *11*, 216–224.
58. Villa, F.; Bagstad, K.J.; Voigt, B.; Johnson, G.W.; Portela, R.; Honzák, M.; Batker, D. A Methodology for Adaptable and Robust Ecosystem Services Assessment. *PLoS ONE* **2014**, *9*, e91001. [CrossRef] [PubMed]
59. Wang, Q.; Wang, Z.; Zhang, H. Impact of anthropogenic aerosols from global, East Asian, and non-East Asian sources on East Asian summer monsoon system. *Atmos. Res.* **2017**, *183*, 224–236. [CrossRef]

60. Fontes, T.; Li, P.; Barros, N.; Zhao, P. Trends of PM2.5 concentrations in China: A long term approach. *J. Environ. Manag.* **2017**, *196*, 719–732. [CrossRef] [PubMed]
61. Yan, T.; Yan, D.R. Analysis on wind feature in Duolun County in Hunshandake Sandy Land. *J. Inn. Mong. For. Sci. Technol.* **2016**, *42*, 21–23, (In Chinese with English Summary).
62. United Nations Environment Programme (UNEP). *Towards a Green Economy: Pathways to Sustainable Development and Poverty Eradication—A Synthesis for Policy Makers*; UNEP: St-Martin-Bellevue, France, 2011.
63. Geijzendorffer, I.R.; Martín-López, B.; Roche, P.K. Improving the identification of mismatches in ecosystem services assessments. *Ecol. Indic.* **2015**, *52*, 320–331. [CrossRef]
64. Baró, F.; Haase, D.; Gómez-Baggethun, E.; Frantzeskaki, N. Mismatches between ecosystem services supply and demand in urban areas: A quantitative assessment in five European cities. *Ecol. Indic.* **2015**, *55*, 146–158. [CrossRef]
65. Duraiappah, A.K.; Asah, S.T.; Brondizio, E.S.; Kosoy, N.; O'Farrell, P.J.; Prieur-Richard, A.-H.; Subramanian, S.M.; Takeuchi, K. Managing the mismatches to provide ecosystem services for human well-being: A conceptual framework for understanding the New Commons. *Curr. Opin. Environ. Sustain.* **2014**, *7*, 94–100. [CrossRef]
66. Egarter Vigl, L.; Depellegrin, D.; Pereira, P.; de Groot, R.; Tappeiner, U. Mapping the ecosystem service delivery chain: Capacity, flow, and demand pertaining to aesthetic experiences in mountain landscapes. *Sci. Total Environ.* **2017**, *574*, 422–436. [CrossRef] [PubMed]
67. Verhagen, W.; Kukkala, A.S.; Moilanen, A.; van Teeffelen, A.J.A.; Verburg, P.H. Use of demand for and spatial flow of ecosystem services to identify priority areas. *Conserv. Biol.* **2017**, *31*, 860–871. [CrossRef] [PubMed]
68. Xie, G.; Cao, S.; Lu, C.; Zhang, C.; Xiao, Y. Current status and future trends for eco-compensation in China. *J. Res. Ecol.* **2015**, *6*, 355–362.